A comparative transport study of Bi2Se3 and Bi2Se3/yttrium iron garnet

Zilong Jiang, Ferhat Katmis, Chi Tang, Peng Wei, Jagadeesh S. Moodera, and Jing Shi

Citation: Applied Physics Letters **104**, 222409 (2014); doi: 10.1063/1.4881975
View online: http://dx.doi.org/10.1063/1.4881975
View Table of Contents: http://scitation.aip.org/content/aip/journal/apl/104/22?ver=pdfcov
Published by the AIP Publishing

A comparative transport study of Bi_2Se_3 and Bi_2Se_3/yttrium iron garnet

Zilong Jiang,[1] Ferhat Katmis,[2] Chi Tang,[1] Peng Wei,[2] Jagadeesh S. Moodera,[2] and Jing Shi[1]
[1]*Department of Physics and Astronomy, University of California, Riverside, California 92521, USA*
[2]*Francis Bitter Magnet Laboratory, Massachusetts Institute of Technology, Cambridge, Massachusetts 02139, USA*

(Received 29 April 2014; accepted 26 May 2014; published online 5 June 2014)

Bilayers of 20 quintuple layer Bi_2Se_3 on 30 nm thick yttrium iron garnet (YIG) have been grown with molecular beam epitaxy in conjunction with pulsed laser deposition. The presence of the ferri-magnetic insulator YIG causes additional scattering to the surface states of the Bi_2Se_3 topological insulator layer, as indicated by the temperature dependence of the resistivity. From the two-channel analysis of the Hall data, we find that the surface contribution in the bilayer samples is greatly reduced. Furthermore, the weak antilocalization effect from the surface states is clearly suppressed due to the presence of the YIG layer. © *2014 AIP Publishing LLC*. [http://dx.doi.org/10.1063/1.4881975]

A spontaneous magnetic order in a topological insulator (TI) breaks the time reversal symmetry in the surface states which can consequently lead to a variety of interesting phenomena such as the quantized anomalous Hall effect (QAHE),[1] magneto-electric effect,[2] and so on. Recently, QAHE has been demonstrated in $Cr_{0.15}(Bi_{0.1}Sb_{0.9})_{1.85}Te_3$ at 30 mK.[3] Another way of introducing the magnetic order in the surface states is to exchange couple a magnetic layer via the proximity effect. To avoid current shunting in transport measurements, a ferro- or ferri-magnetic insulator (FMI) is required. This approach has recently been pursued using EuS[4,5] and GdN[6] FMI materials. Yttrium iron garnet (YIG) is a promising FMI for its high Curie temperature (~550 K), chemical and magnetic stability, and large insulating band gap (~2.85 eV). Recently, high-quality YIG has been incorporated in other bilayer structures for investigating spin current effects[7,8] and magnetic proximity effect.[9,10] In this work, we report our transport study of Bi_2Se_3, a well-studied TI material, grown on YIG.

YIG films of ~30 nm thick are grown on (110) gadolinium gallium garnet (GGG) substrates at ~700 °C using a pulsed layer deposition (PLD) system. The layer-by-layer growth mode can be achieved as indicated by the reflection high-energy electron diffraction (RHEED) intensity oscillations during growth.[10] In general, YIG has an epitaxial relationship with the GGG substrate as indicated by the RHEED pattern. To develop a strong proximity effect across the interface in hybrid structures, a smooth and clean interface is critically important. Fig. 1(a) is an atomic force microscopy (AFM) image of a typical 30 nm thick YIG film. On flat terraces, the mean roughness is ~0.6 Å. The terraces are separated with steps of 4.5 Å in height, indicating atomic steps between adjacent (110) planes of YIG. We also grow several YIG films on Si (001) substrates under the same growth conditions. YIG films on Si are polycrystalline, but the mean roughness is ~1 Å. Magnetization measurements with the magnetic field oriented in both in-plane and out-of-plane directions are taken with a vibrating sample magnetometer system at room temperature (Fig. 1(b)), which indicate well-defined in-plane magnetic anisotropy. In TI/FMI hybrid structures, even though strong exchange coupling may exist across the interface, no gap in the topological surface states of TI is expected with an in-plane magnetization.[11,12] Therefore, an out-of-plane external magnetic field is necessary to orient the magnetization of TI/YIG perpendicular to the film. Ferromagnetic resonance (FMR) linewidth and resonance field characterize the quality of magnetic films which are related to the damping and average magnetization M_s. The average FMR linewidth ΔH of our PLD grown films is ~10 Oe and can be as narrow as ~3.5 Oe (Fig. 1(c)). $4\pi M_s$ obtained from the resonance field ranges from 2000 to 2480 Oe. These results indicate excellent magnetic properties of our PLD-grown YIG films.

To grow Bi_2Se_3/YIG hybrid structures, the YIG films are transferred to an ultra-high vacuum (low 10^{-10} Torr) molecular beam epitaxy chamber for the Bi_2Se_3 growth. To

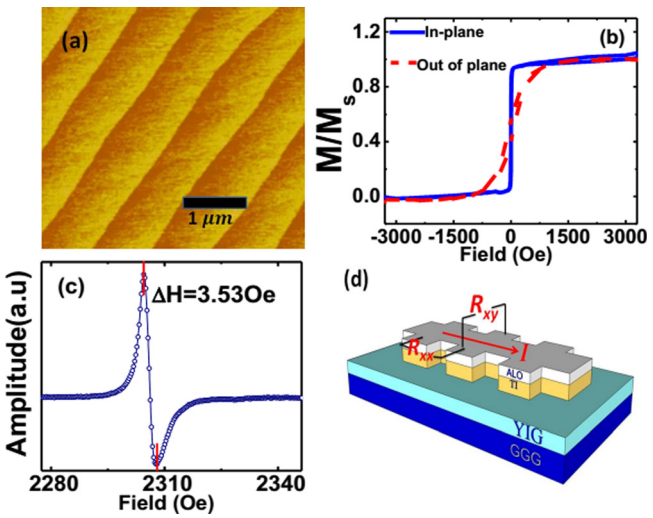

FIG. 1. (a) AFM image of a representative ~30 nm YIG thin film. (b) Normalized magnetic hysteresis loops at 300 K of a YIG/GGG film with an applied field in-plane ($H_{\parallel}$) and out-of-plane ($H_{\perp}$). (c) FMR spectrum of a ~30 nm thick YIG on GGG. (d) Schematic diagram of the patterned Hall bar hybrid structure (Bi_2Se_3/YIG) and notations for transport measurement. R_{xx} and R_{xy} refer to sheet resistance and hall resistance, respectively.

ensure good interface quality, *in-situ* oxygen plasma cleaning is performed to remove organic contaminants on YIG before the growth. High-purity (5N) elemental Bi and Se are co-evaporated from different Knudsen-cells with typical growth rates between 0.5 and 1 nm/min, determined by *in-situ* quartz crystal micro balance. The thickness is confirmed by *ex-situ* x-ray reflectivity measurements. The temperature of the substrate is kept at $300 \pm 5\,^{\circ}C$ for crystalline Bi_2Se_3 growth, i.e., in the epitaxial growth regime with a hexagon-on-cube orientation. After that, a 5 nm Al_2O_3 is deposited as a capping layer. Two control samples of 20 quintuple layer (QL) Bi_2Se_3 capped with Al_2O_3 are grown on Si simultaneously. Hereafter, we refer Bi_2Se_3/YIG/GGG and Bi_2Se_3/YIG/Si samples as the bilayers and Bi_2Se_3/Si as the control sample. In this work, we report transport results in two Bi_2Se_3 (20 QL)/YIG/GGG samples grown in nominally the same conditions, one Bi_2Se_3 (20 QL)/YIG/Si and two Bi_2Se_3 (20 QL)/Si control samples.

To characterize the crystal structure, x-ray diffraction (XRD) is performed with a high-resolution x-ray diffractometer using $CuK_{\alpha 1}$ radiation (wavelength $\lambda = 1.54056$ Å) over a wide diffraction angle range. Combination of different types of scans is performed in order to investigate the crystallographic relationship between substrate and grown layer. Wide range out-of-plane XRD scans reveal that the Bi_2Se_3/YIG thin film consists of a single Bi_2Se_3 phase and a couple of textured YIG phases (Fig. 2(a)). In the figure, the TI layer shows the (00*l*) type reflections along the growth direction. The Bragg peak positions of Bi_2Se_3 agree in all

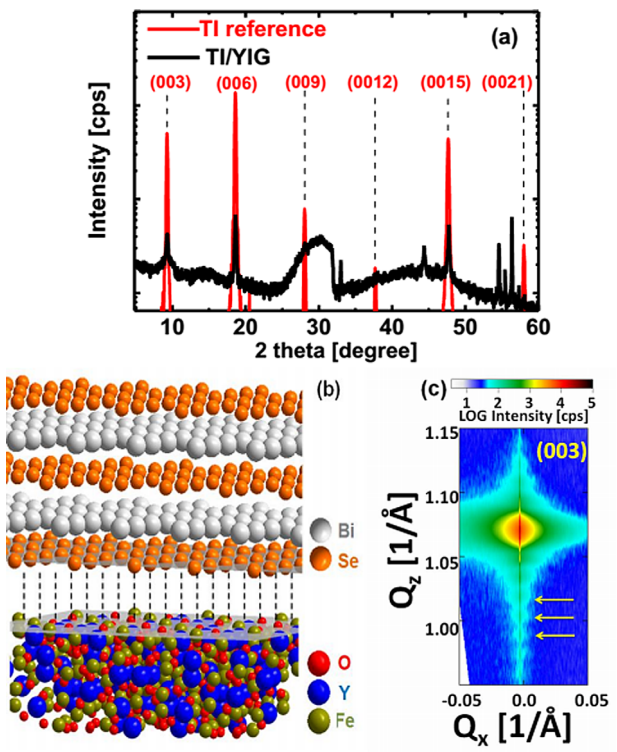

FIG. 2. XRD analysis for Bi_2Se_3/YIG heterostructure is shown. (a) Wide angle ω-2θ-scan on simultaneously grown Bi_2Se_3 layer and Bi_2Se_3/YIG heterostructures. The TI layer has the (00*l*) type reflections along the growth direction. (b) Illustration of Bi_2Se_3/YIG heterostructure. (c) High resolution XRD reciprocal space mapping at the vicinity of the Bragg peak for symmetric (003).

samples, which indicate that 20 QL of Bi_2Se_3 films are thick enough to relax back to the bulk lattice structure regardless of the substrates they are grown on. Fig. 2(c) shows a reciprocal space map of the *k-l* cut at the vicinity of (003) Bragg peak of a Bi_2Se_3 (20 QL)/YIG. Strong Kiessig fringes are observed around the diffraction peak, indicating good Bi_2Se_3 surface and Bi_2Se_3/YIG interface correlation and homogeneous growth of Bi_2Se_3. All samples show similar features in XRD mapping, which indicate excellent structural quality of TI on YIG.

For transport measurements, the bilayer samples (Bi_2Se_3/YIG) are patterned into Hall bar structures (channel width of 100 μm and length of 900 μm) by standard photolithography and etched by Ar plasma. The Au/Ti contact pads are deposited by an electron beam-evaporator. The four-terminal transport measurements are taken in a physical property measurement system over the temperature range of 1.9–300 K and in magnetic fields up to 14 T.

Fig. 3(a) shows the sheet resistance vs. temperature curves for four samples: three bilayer samples and one control sample. At high temperatures, they all show a metallic behavior, i.e., with positive temperature coefficients. Although they have approximately the same temperature coefficient in resistance, the bilayer samples clearly have larger sheet resistance, or suppressed conductivity compared with the control sample. The resistance of Bi_2Se_3/YIG/Si (sample #1) is the highest, followed by the two Bi_2Se_3/YIG/GGG samples (#2 and #3). We note that the resistance curves of samples #2 and #3 are not the same although they are grown under nominally the same conditions. Below 20 K, however, the resistance has a minimum and starts to increases as the temperature decreases. A comparison of the low-temperature insulating behaviors of all samples is shown in the inset of Fig. 3(a), and it is clear that the insulating behavior is more pronounced in the bilayer samples. The onset temperature of the insulating behavior is also higher in bilayer samples. These results suggest that the presence of the magnetic layer may be responsible for the stronger insulating behavior in the bilayer samples.[5,13]

The Hall effect measurements indicate that charge carriers of Bi_2Se_3 in all samples are of n-type with a net carrier density $\sim 4 \times 10^{19}/cm^3$ which does not vary significantly (from 3.7×10^{19} to $4.4 \times 10^{19}/cm^3$) among the four samples. Fig. 3(b) shows a comparison of the Hall conductance, G_{xy}, between the control sample and a bilayer sample (#3). The non-linear G_{xy} in the control sample suggests the co-existence of more than one type of carriers. Similar non-linear Hall data are also found in other TI materials and attributed to the transport of both surface and bulk carriers.[14–16] However, the non-linear Hall effect is strongly suppressed in the bilayer samples with the inserted YIG magnetic layer, suggesting one type of carriers dominating the transport. We assume that only the surface channel in the bilayer samples is affected due to the presence of the adjacent YIG layer, which gives rise to the nearly linear Hall conductance dominated by the bulk carriers. To find out the mobility and carrier density for corresponding channels, we do the two-band fitting[15] to our Hall conductance data in both control and bilayer samples

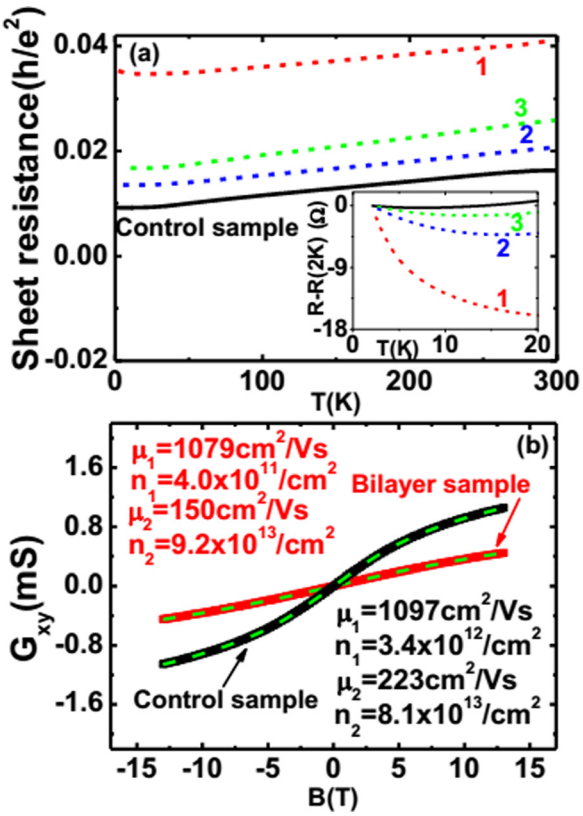

FIG. 3. Resistance vs. temperature and Hall effect. (a) Temperature dependent sheet resistances for one control sample (solid line) and three bilayer samples (Bi_2Se_3/YIG, dashed lines). The insulating behavior (<20 K) is enhanced in bilayer samples (inset). (b) Two-band fitting for the Hall conductance of control sample and bilayer sample #3. The mobilities and corresponding carrier densities from the fitting are noted in the figure.

$$G_{xy}(B) = eB\left(\frac{C_1\mu_1 - C_2}{\left(\frac{\mu_1}{\mu_2}-1\right)\left(1+\mu_2^2B^2\right)} + \frac{C_1\mu_2 - C_2}{\left(\frac{\mu_2}{\mu_1}-1\right)\left(1+\mu_1^2B^2\right)}\right), \quad (1)$$

where B is the applied magnetic field in the perpendicular direction, μ_1 and μ_2 are the carrier mobilities of two channels, n_1 and n_2 are the carrier densities of two channels, and $C_1 = n_1\mu_1 + n_2\mu_2 = \frac{G_{xx}(0)}{e}$ and $C_2 = n_1\mu_1^2 + n_2\mu_2^2 = \lim_{B\to 0}\frac{G_{xy}(B)}{eB}$ are combinations of the carrier density and mobility in two channels and can be obtained directly from the longitudinal and Hall data, i.e., G_{xx} and G_{xy}. The fitting results are displayed in the figure. The mobility of channel one is at least a factor of 5 higher than that of channel two, and it is not affected by the presence of YIG. However, the density of this channel is decreased dramatically in the bilayer sample. On the other hand, both the mobility and carrier density of channel two do not change significantly after inserting the YIG layer. Hence, we assign channel one as the surface channel and channel two as the bulk channel, respectively. Clearly, the surface channel has higher carrier mobility than the bulk channel. In the meantime, we find that the 2D carrier density of the surface channel of the bilayer sample ($n_{surface} = 4.0 \times 10^{11}/\text{cm}^2$) decreases by one order of magnitude compared with that of the control sample ($n_{surface} = 3.4 \times 10^{12}/\text{cm}^2$). Similar effects are found in other bilayer samples, confirming that the surface channel of Bi_2Se_3 is affected by the presence of an insulating magnetic layer.

Fig. 4(a) shows the normalized magneto-resistance (MR) data at 1.9 K for all samples taken under a perpendicular field from −13 to 13 T. They have overall positive MR up to 13 T, but the high-field MR curve of the control sample (solid) is well separated from those of the 3 bilayer samples (dashed). The high-field positive MR trend is reduced in the bilayer samples. Fig. 4(b) shows the low-field magneto-conductance (MC) data in the low-field region of the MR data in Fig. 4(a). The cusp-like MC data are normally attributed to the weak anti-localization (WAL) effect in materials with strong spin-orbit coupling. Clearly, our data show that the WAL effect in Bi_2Se_3 is suppressed by being placed in proximity with YIG as seen in Fe/TI devices.[17] To understand the origin of the weakened WAL cusp in the bilayer samples, we carry out a quantitative analysis of low-field MC data. In Fig. 4(b), the low-field MC is defined as $\Delta\sigma(\text{B}) = \Delta\sigma_{xx}(\text{B}) - \Delta\sigma_{xx}(0)$. We adopt the Hikami-Larkin-Nagaoka (HLN) theory to fit the MC data. In the limit that the inelastic scattering time is much longer than both the elastic and spin-orbit scattering times, the field dependent conductance is described by the HLN theory[18] as

$$\delta\sigma(\text{B}) = \sigma(\text{B}) - \sigma(0) = \frac{\alpha e^2}{2\pi^2\hbar}\left[\Psi\left(\frac{1}{2}+\frac{\hbar}{4eBl_\phi^2}\right) - \ln\left(\frac{\hbar}{4eBl_\phi^2}\right)\right], \quad (2)$$

where l_ϕ is the phase coherence length, ψ is the digamma function, and α is a coefficient determined by the type of localization. In the absence of magnetic scattering, α has a value of −0.5 (symplectic case), which is the prefactor for the pure WAL with single coherent channel. In the case of magnetic scattering, $\alpha = 0$, namely, the unitary group. However, the weak localization-like MC has a prefactor of 0.5. The MC of the control Bi_2Se_3 sample can be fitted very well with $\alpha = 0.5$, which is confirmed in another control Bi_2Se_3 sample (20 QL) (lower left circle in Fig. 4(c)). Previously reported α values in Bi_2Se_3 samples with different thicknesses (≥5 QL) were also found to be distributed over a narrow range near −0.5.[19–21] Our observations in the control samples are consistent with those experiments. However, the α values of the bilayer samples (#1, #2, and #3) are in the range of −0.25 to −0.35, consistently smaller in magnitude than those of the control samples (Fig. 4(c)). Clearly, the bilayer samples distinguish themselves from the control samples in term of the α value, suggesting a trend transitioning towards the unitary class from the symplectic class as a consequence of more magnetic scattering.[12,17] In Bi_2Se_3/YIG/Si, since there is likely more spin disorder in polycrystalline YIG, the stronger magnetic scattering may be responsible for the most reduced α value.

Fig. 4(d) shows a temperature dependent low-field MC for bilayer sample #3. The thermal broadening of the negative MC reduces the WAL effect quickly as the temperature increases, which is reflected in the decreasing α value from the HLN fitting (Fig. 4(e), upper curve). Such a trend slows down and approaches saturation below 10 K. The α value extracted for the control sample shows a similar trend[6,25] but

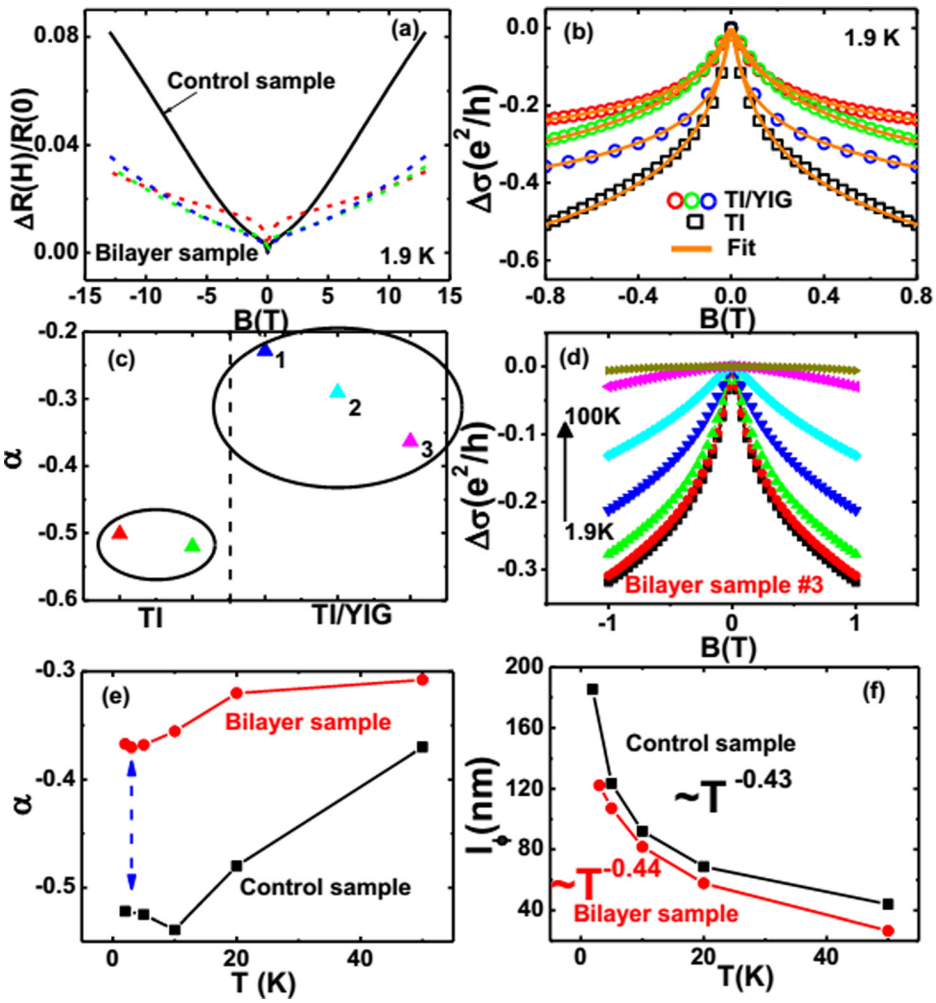

FIG. 4. Magnetoresistance of control sample and bilayer samples. (a) Normalized MR ratio of control sample (solid) and bilayer samples (dashed) in high fields. (b) MC of control sample (squares) and bilayer samples (circles) with fits (solid lines) at 1.9 K in the low field region. (c) The obtained HLN fitting parameter α from (b) for both the control and bilayer samples. The prefactor α of 3 bilayer samples (right circle) is clearly above that of control sample (left circle). (d) Temperature dependent low-field MC of bilayer sample #3 from 1.9 K to 100 K. (e) Temperature dependent prefactor α for the bilayer #3 (upper) and control samples (lower). (f) Temperature dependence of the phase coherence length l_ϕ for the control sample (upper) and bilayer sample #3 (lower).

remains larger in magnitude than that of the bilayer sample (Fig. 4(e), lower curve). The gap between these two curves is the largest at the lowest temperature and decreases steeply at high temperatures.

Fig. 4(f) shows the temperature dependence of the coherence length l_ϕ in the control sample and bilayer sample #3 extracted using Eq. (2). Theoretically, the coherence length is proportional to $T^{-1/2}$ and $T^{-3/4}$ for 2D and 3D systems, respectively.[22] The monotonic decrease of the coherence length as the temperature increases is observed in both bilayer sample #3 (lower) and the control Bi_2Se_3 sample (upper), similar to other TI systems.[23–25] The fitting gives $l_\phi = T^{-0.44}$ for bilayer sample #3 and $l_\phi = T^{-0.43}$ for the control sample, suggesting WAL at low fields originates from the 2D surface states. Moreover, we notice here that the phase coherence length for Bi_2Se_3/YIG bilayer sample is smaller than that for Bi_2Se_3 control sample, especially at low temperatures. For example, in 1.9 K, the l_ϕ for bilayer sample #3 is 129 nm which is obviously smaller than that of the pure Bi_2Se_3 (190–350 nm).[17,21,25] The reduction of the coherence length l_ϕ in the bilayer sample is probably caused by additional inelastic scattering such as electron-magnon scattering to the topological insulator surface states next to the magnetic layer.[12,17]

In summary, our transport results in Bi_2Se_3/YIG bilayer structures indicate strong suppression of the surface transport channel as well as the weak antilocalization in the topological surface states. We attribute these transport phenomena to the increased magnetic scattering at the TI/FMI interface. A stronger magnetic proximity effect is expected in bilayers with a thinner and more insulating TI layer.

Work at UCR was supported by a UC-Lab grant and by NSF-ECCS (#1202559). Work at MIT was supported by the NSF Grant No. DMR-0819762 through the MRSEC Program, the NSF Grant No. DMR-1207469, the ONR Grant No. N00014-13-1-0301, and the NSF Grant No. DMR-1231319 through the STC Center for Integrated Quantum Materials. Part of this work was carried out at the MIT-CMSE shared experimental facilities. We would also like to thank Vivek Aji and Ward Beyermann for helpful discussions.

[1]R. Yu, W. Zhang, H.-J. Zhang, S.-C. Zhang, X. Dai, and Z. Fang, Science **329**, 61 (2010).
[2]A. M. Essin, J. E. Moore, and D. Vanderbilt, Phys. Rev. Lett. **102**, 146805 (2009).
[3]C.-Z. Chang, J. Zhang, X. Feng, J. Shen, Z. Zhang, M. Guo, K. Li, Y. Qu, P. Wei, and L.-L. Wang *et al.*, Science **340**, 167 (2013).
[4]P. Wei, F. Katmis, B. A. Assaf, H. Steinberg, P. JarilloHerrero, D. Heiman, and J. S. Moodera, Phys. Rev. Lett. **110**, 186807 (2013).
[5]Q. I. Yang, M. Dolev, L. Zhang, J. Zhao, A. D. Fried, E. Schemm, M. Liu, A. Palevski, A. F. Marshall, S. H. Risbud, and A. Kapitulnik, Phys. Rev. B **88**, 081407 (2013).
[6]A. Kandala, A. Richardella, D. W. Rench, D. M. Zhang, T. C. Flanagan, and N. Samarth, Appl. Phys. Lett. **103**, 202409 (2013).

[7]B. Heinrich, C. Burrowes, E. Montoya, B. Kardasz, E. Girt, Y.-Y. Song, Y. Sun, and M. Wu, Phys. Rev. Lett. **107**, 066604 (2011).
[8]D. Qu, S. Y. Huang, J. Hu, R. Wu, and C. L. Chien, Phys. Rev. Lett. **110**, 067206 (2013).
[9]S. Y. Huang, X. Fan, D. Qu, Y. P. Chen, W. G. Wang, J. Wu, T. Y. Chen, J. Q. Xiao, and C. L. Chien, Phys. Rev. Lett. **109**, 107204 (2012).
[10]T. Lin, C. Tang, and J. Shi, Appl. Phys. Lett. **103**, 132407 (2013).
[11]X.-L. Qi, T. L. Hughes, and S.-C. Zhang, Phys. Rev. B **78**, 195424 (2008).
[12]H.-Z. Lu, J.-R. Shi, and S.-Q. Shen, Phys. Rev. Lett. **107**, 076801 (2011).
[13]M. Liu, J. Zhang, C.-Z. Chang, Z. Zhang, X. Feng, K. Li, K. He, L.-l. Wang, X. Chen, X. Dai, Z. Fang, Q.-K. Xue, X. Ma, and Y. Wang, Phys. Rev. Lett. **108**, 036805 (2012).
[14]Z. Ren, A. A. Taskin, S. Sasaki, K. Segawa, and Y. Ando, Phys. Rev. B **82**, 241306(R) (2010).
[15]N. Bansal, Y. Kim, M. Brahlek, E. Edrey, and S. Oh, Phys. Rev. Lett. **109**, 116804 (2012).
[16]A. A. Taskin, Z. Ren, S. Sasaki, K. Segawa, and Y. Ando, Phys. Rev. Lett. **107**, 016801 (2011).
[17]H.-T. He, G. Wang, T. Zhang, I.-K. Sou, G. K. L. Wang, and J.-N. Wang, Phys. Rev. Lett. **106**, 166805 (2011).
[18]S. Hikami, A. Larkin, and Y. Nagaoka, Prog. Theor. Phys. **63**, 707 (1980).
[19]A. A. Taskin, S. Sasaki, K. Segawa, and Y. Ando, Phys. Rev. Lett. **109**, 066803 (2012).
[20]J. Chen, X. Y. He, K. H. Wu, Z. Q. Ji, L. Lu, J. R. Shi, J. H. Smet, and Y. Q. Li, Phys. Rev. B **83**, 241304(R) (2011).
[21]Y. Kim, M. Brahlek, N. Bansal, E. Edrey, G. A. Kapilevich, K. Iida, M. Tanimura, Y. Horibe, S.-W. Cheong, and S. Oh, Phys. Rev. B **84**, 073109 (2011).
[22]B. L. Altshuler, A. G. Aronov, and D. E. Khmelnitskii, J. Phys. C: Solid State Phys. **15**, 7367 (1982).
[23]S. Matsuo, T. Koyama, K. Shimamura, T. Arakawa, Y. Nishihara, D. Chiba, K. Kobayashi, T. Ono, C.-Z. Chang, K. He *et al.*, Phys. Rev. B **85**, 075440 (2012).
[24]L. Bao, L. He, N. Meyer, X. Kou, P. Zhang, Z. Chen, A. V. Fedorov, J. Zou, T. M. Riedemann, T. A. Lograsso *et al.*, Sci. Rep. **2**, 726 (2012).
[25]H. Steinberg, J.-B. Laloe, V. Fatemi, J. S. Moodera, and P. Jarillo-Herrero. Phys. Rev. B **84**, 233101 (2011).